

Silica-Encapsulated Efficient and Stable Si Quantum Dots with High Biocompatibility

G. Amato

Received: 2 March 2010/Accepted: 17 April 2010/Published online: 1 May 2010
© The Author(s) 2010. This article is published with open access at Springerlink.com

Abstract A facile fabrication method to produce biocompatible semiconductor Quantum Dots encapsulated in high quality and thick thermal oxide is presented. The process employs sonication of porous Si/SiO₂ structures to produce flakes with dimension in the 50–200 nm range. These flakes show a coral-like SiO₂ skeleton with Si nanocrystals embedded in and are suitable for functionalization with other diagnostic or therapeutic agents. Silicon is a biocompatible material, efficiently cleared from the human body. The Photoluminescence emission falls in the transparency window for living tissues and is found to be bright and stable for hours in the aggressive biological environment.

Keywords Semiconductor · Quantum Dots · Nanocrystals · Fabrication · Clearance · Photoluminescence

Introduction

The production of functional nanomaterials for therapeutic and diagnostic purposes is one of the major challenges of nowadays nanotechnology [1, 2]. The intrinsic properties of such nanostructures, say, the efficient photoluminescence [3, 4], the strong superparamagnetism [5], or the characteristic Raman signatures [6], combined with the large specific capacity for drug loading [7] allow to forecast wide application in the biological and medical fields. However, the size and charge of most nanoparticles preclude their efficient clearance from the body as intact

nanoparticles. Without such clearance or their biodegradation into biologically benign components, toxicity is potentially amplified [8]. On the other hand, rapid renal excretion [8], observed with particle diameters <5.5 nm, is often undesirable because the relatively short residence time do not allow the nanoparticles to carry out their action.

This discussion points out on the importance of the nanoparticles engineering in terms of size and composition but also addresses on the rates of self-destruction and the formation of non-toxic, renally cleared products.

Among the various kinds of functional nanomaterials, semiconductor Quantum Dots (QD) received particular attention [3, 4, 9]. These are nanoparticles in which charge carriers are three-dimensionally confined. The quantum confinement provides size-tunable absorption bands and emission color to QDs. The photoluminescence (PL) of QDs is exceptionally bright and stable, with very narrow emission but broad absorption spectra, making them potential candidates for biomedical imaging and therapeutic interventions, but concerns persist about their safety [10]. Most toxicology data are derived from in vitro studies and may not reflect in vivo responses, so the fear of toxicity greatly prevented their employment in studies in vivo. Encapsulation in SiO₂ shells [4, 11, 12] is a promising approach for biophotonic applications where hydrophilicity, biocompatibility, and low rates of self-destruction are needed.

In the present scenario, an interesting possibility is offered by Si QDs. Silicon is well known as a biocompatible material [13], widely used in nanomedicine [14] or in bone growth [15]. In Si nanocrystals with diameter down to 1–3 nm, the exciton quantum confinement is the mechanism at the base of the bright, visible photoluminescence [16]. This effect is easily observed in Porous

G. Amato (✉)
Quantum Research Laboratory, INRIM, strada delle Cacce 91,
10135 Turin, Italy
e-mail: g.amato@inrim.it

Silicon (PS), obtained either by electrochemical etching of high-resistivity p-type substrates [17] or by stain etching [18]. The energy position and FWHM of the PL spectrum is related to the average size and dispersion of the nanoparticles composing the PS nanospunge [19]. Moreover, the electrical behavior of PS can be tuned from insulating to semiconducting (p-, or n-type), independently on the doping type and level of the starting substrate [20].

A recent paper [21] reports on the use of Si nanoparticles, derived from luminescent PS, as biodegradable optical markers and drug delivery agents. The investigated Si nanoparticles have diameters of 100–200 nm and are agglomerates of single luminescent nanocrystals. PL is centered in the near-IR and quite stable, thanks to oxidation during activation of PL in aqueous solution. Such a structure is particularly interesting for two reasons. First, it avoids renal filtration, prolonging the residence time in the living body; second, its porous structure, reminiscent of the pristine PS, allows for incorporation of drugs and for their slow release.

In the present paper, an alternative method to achieve efficient SiO_2 encapsulation, with more durable PL and lower degradation in biological solution, is presented.

Experimental

Materials and Methods

The starting PS samples are obtained by anodizing p⁺ substrates ($1 \text{ m}\Omega \text{ cm}$, <100> oriented). Such material is well known to be composed by nanocrystals with average dimension $>10 \text{ nm}$, somewhat smaller in high-porosity samples. As a consequence for the weak excitonic confinement, the resulting PS is poorly photoluminescent. It has been demonstrated, however, that oxidation in dry O_2 at 1000°C greatly enhances the PL, with intensity comparable to conventional PS from p-type substrates [22]. This is related to the controlled growth of the SiO_2 shell which reduces the Si core to a few nm and to the superior passivating properties of the thermal oxide. In fact, thermal oxide is well known [23] to be nearly stoichiometric, and the spin density at the Si/ SiO_2 interface has been evaluated to be small [22].

Oxide Growth

The PS samples have been oxidized in an horizontal quartz tube at O_2 atmospheric pressure. A first, pre-oxidation step at 300°C has been carried out in order to reduce surface Si atoms mobility, preventing in this way the structure collapse at the oxidation temperature (1000°C).

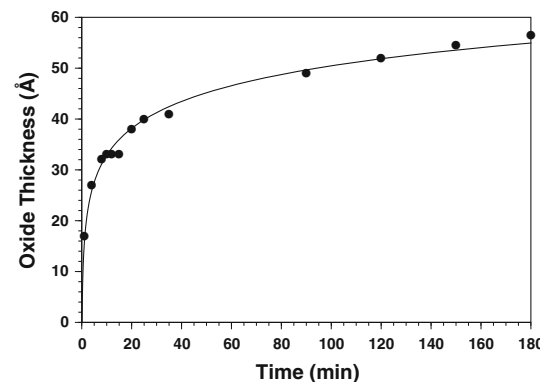


Fig. 1 Oxide thickness on a 60% porosity PS layer, as a function of oxidation time, calculated according to ref. [22]

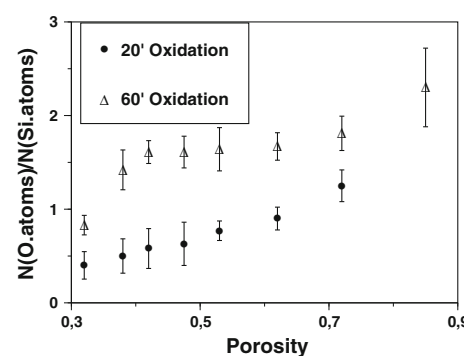


Fig. 2 O/Si ratio, as a function of the sample porosity, for two different oxidation times

Figure 1 reports the thickness of the SiO_2 shell, as extracted by analyzing gravimetric data taken from a PS sample with 60% porosity [20]. A AND microbalance with 10^{-5} g sensitivity has been used for the purpose. The saturation at about 5 nm is related to the full conversion of Si crystallites (10 nm average diameter) into SiO_2 . In Fig. 2, the gravimetric data are displayed showing the O/Si ratio as a function of porosity for two oxidation times. A saturated value of $\text{O/Si} = 2$ is reached upon the total conversion of the Si skeleton into SiO_2 . The comparison of the two graphs allows to predict both the Si core diameter and the thickness of the SiO_2 shell by a proper choice of the sample porosity and oxidation duration. For the present work, porosity varied between 40 and 60%, whereas oxidation duration was in the 10–40 min range.

PS Structuring

Because of the low samples porosity and the high degree of oxidation, the volume expansion due to Si conversion into SiO_2 cannot be neglected. In fact, the pore coalescence has been reported [22]: this effect, especially for the lower porosities prevents O_2 molecules diffusion and fixation into

the pores. Of course, this is detrimental to the QD passivation. To circumvent this problem, we produced PS multilayers by alternating 40-nm LP (low porosity) and 40-nm HP (high porosity) layers, by means of periodic variations of the anodizing current in the aqueous HF/ethanol electrolyte. As an example, 100 periods comprising steps of $10/220 \text{ mA cm}^{-2}$ were applied by means of a Keithley 2400 programmable current source. Samples have been cleaved before oxidation. The HP layers act as channels for lateral O₂ diffusion into the porous structure, allowing for the uniform oxidation of the LP layers.

Nanoparticle Production

The samples were then sonicated for 6–8 h in toluene, obtaining a suspension composed by two classes of nanoparticles. The first class of <10 nm SiO₂ particles derives from the HP layers, whereas the second class is composed by Si/SiO₂ *nanoflakes* originating from LP regions. The dimension of such *nanoflakes* ranges from 50 to 300 nm and can be separated by the SiO₂ nanoparticles by means of a 20-nm membrane filter. A second filtration step, using a 200-nm membrane, allows for further size selection of the Si/SiO₂ *nanoflakes*.

Characterization Results

Electron Microscopy

The typical structure of a large (>300 nm) Si/SiO₂ *nanoflake* is shown in Fig. 3. The TEM micrograph shows darker, nearly spherical dots, i.e., the Si nanocrystals, embedded in the SiO₂ matrix. Both the thickness of this encapsulating film and the Si QDs diameter are consistent with the previous evaluations. The bright spots and the halo in the diffraction pattern reported in the inset indicates the presence of both amorphous (SiO₂) and crystalline (Si) phases. The magnified view confirms the crystallinity of the Si nanodots.

Interesting features of the *nanoflakes* obtained in this way are the coral-like structure and the large specific surface. Both can be fruitfully employed to add further functionalities, e.g., embedded magnetic nanodots, drugs, and other fluorophores.

Photoluminescence

By means of a Scientech monochromator with f/4.5 aperture, equipped with an EG&G cooled multichannel detector, the PL emitted by Si/SiO₂ *nanoflakes* under Hg illumination has been analyzed.

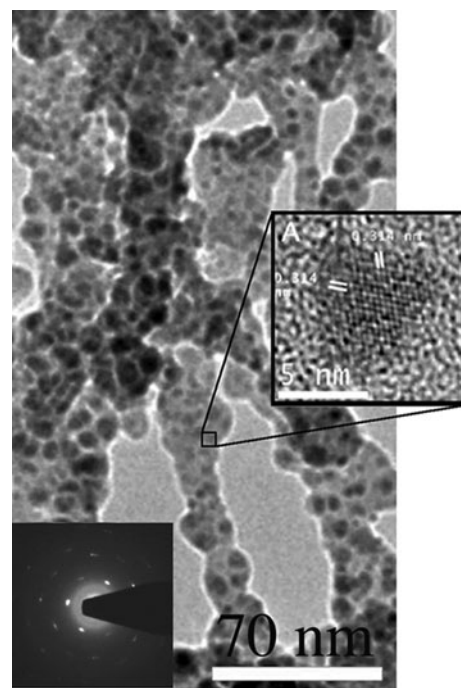


Fig. 3 TEM Micrograph of a Si/SiO₂ *nanoflake*, with maximum axis >300 nm, showing the coral-like structure and the encapsulated Si nanodots. Insets shows the electron diffraction pattern (left bottom), and a magnified image of the Si nanodots structure (A)

Light emission is centered in the near-IR, as shown in Fig. 4, and exceptionally stable in ambient conditions, being unaltered after 2 weeks of air exposure.

The PL stability is obviously crucial when QDs are incubated into biological systems. This test has been carried out by immersing the *nanoflakes* into a PBS (phosphate-buffered saline) solution at $T = 37^\circ\text{C}$ and pH = 7.5. The PL color remains dark red and the intensity reduces to 60% in about 4 h of incubation, a very different behavior respect to [21], where the optical emission is reported to start decreasing just after incubation. After 4 h of

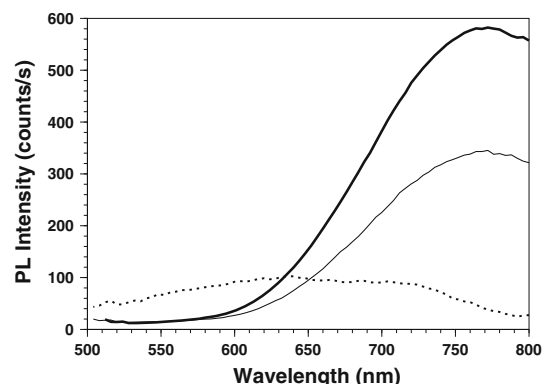


Fig. 4 PL spectra from Si/SiO₂ *nanoflakes*. Bold line shows the emission spectrum before incubation in PBS. Thin line: after 240-min incubation time. Dashed spectrum is collected after 270-min incubation time

incubation, the QDs emission blue-shifts and decreases more abruptly, consistently to what reported in [21]. This different behavior is easily explained in terms of thickness and quality of the SiO_2 encapsulation. In the present case, the very thick silica layer is hardly consumed by the PBS solution, whereas the following PL quenching and blue-shifting are signatures for the consumption of the Si fluorophores.

Biocompatibility

There are several reports about the biocompatibility of Si nanostructures, most of them related to the PS itself which is a particularly interesting material in the present case, since our *nanoflakes* directly derive from it. First biocompatibility tests were carried out a decade ago [24], and more recently, implants of PS into living tissues have been carried out, without the observation of any inflammatory reactions [25].

It is well known, on the other hand, that Si is a common trace element in humans, and a biodegradation product of porous silicon, orthosilicic acid ($\text{Si}(\text{OH})_4$), is the form predominantly absorbed by humans and is naturally found in numerous tissues [26].

Silicic acid release from the dots was measured by placing the nanoflakes into a specified volume of PBS and fitting a screw-cap to ensure the volume was sealed. Samples of the incubating solution were taken at 1-day intervals, measuring 400 μl . Data have been compared with those taken from a c-Si sample and an untreated PS membrane.

Analysis was by a molybdenum (molybdate) blue assay, in which ammonium molybdate in solution reacts with silicic acid in the sample to form silicomolybdic acid (yellow) which is subsequently reduced to form a molybdate blue complex with a peak absorbance at 810 nm. Silicic acid concentration standards were prepared with sodium metasilicate pentahydrate analysis.

The data reported in Fig. 5 show the relatively slow release of $\text{Si}(\text{OH})_4$ from oxidized *nanoflakes*, compared with unoxidized PS. Saturation occurring after 3 days for *nanoflakes* is related to the full consumption of sample's mass, which is considerably lower than in the other two cases.

It seems that, at the present level of investigation, a possible toxic effect of Si nanodots could be related with O_2 radicals, as proposed by Fujioka et al. [27]. It has to be stressed, however, that those authors observed such cytotoxic effect only at high concentration.

Conclusions

The method here described allows for producing very stable and efficient Si-based fluorophores, with improved

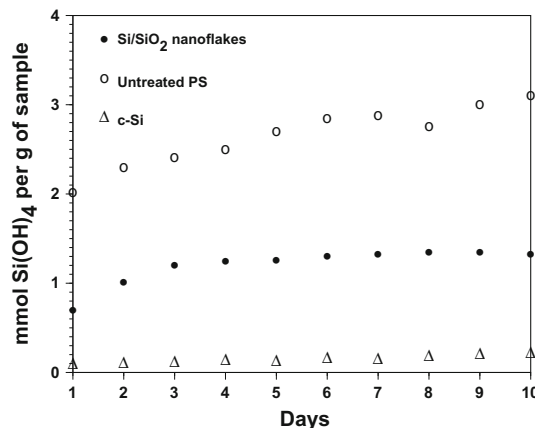


Fig. 5 Silicic acid release from three different Si samples in PBS solution. See text for details

resistance to biological agents, and emitting in the near-IR window for light transmission of living tissues. Si/SiO_2 *nanoflakes* selected in the 50–200 nm range do not undergo the renal filtration, whereas silica encapsulation allows long residence times in the living body, a necessary condition for the nanoparticles to carry out their action. The coral-like structure of the *nanoflakes* allows for the incorporation of other diagnostic and therapeutic agents.

Acknowledgments Work supported by the Piedmont Region through the CIPE 2004-D29 Project.

Open Access This article is distributed under the terms of the Creative Commons Attribution Noncommercial License which permits any noncommercial use, distribution, and reproduction in any medium, provided the original author(s) and source are credited.

References

1. C.-X. Liu, Nano Biomed. Eng. **1**, 1–18 (2009)
2. D. Cui, Y. Han, Z. Li, H. Song, K. Wang, R. He, B. Liu, H. Liu, C. Bao, P. Huang, J. Ruan, F. Gao, H. Yang, H.S. Cho, Q. Ren, D. Shi, Nano Biomed. Eng. **1**, 94–112 (2009)
3. V. Biju, S. Mundayoor, R.V. Omkumar, A. Anas, M. Ishikawa, Biotechnol. Adv. **28**, 199–213 (2010)
4. R. Han, M. Yu, Q. Zheng, L. Wang, Y. Hong, Y. Sha, Langmuir ACS J. Surf. Colloids **25**, 12250–12255 (2009)
5. P. Lee, S. Hsu, J. Wang, J. Tsai, K. Lin, S. Wey, F. Chen, C. Lai, T. Yen, H. Sung, Biomaterials **31**, 1316–1324 (2010)
6. Z. Chen, S.M. Tabakman, A.P. Goodwin, M.G. Kattah, D. Daranciang, X. Wang, G. Zhang, X. Li, Z. Liu, P.J. Utz, K. Jiang, S. Fan, H. Dai, Nat. Biotech. **26**, 1285–1292 (2008)
7. R. Vishwanathan, T.A. Wilson, R.J. Nicolosi, Nano Biomed. Eng. **1**, 57–73 (2009)
8. H. Soo Choi, W. Liu, P. Misra, E. Tanaka, J.P. Zimmer, B. Itty Ipe, M.G. Bawendi, J.V. Frangioni, Nat. Biotech. **25**, 1165–1170 (2007)
9. W.W. Yu, E. Chang, R. Drezek, V.L. Colvin, Biochem. Biophys. Res. Comm. **348**, 781–786 (2006)

10. T.S. Hauck, R.E. Anderson, H.C. Fischer, S. Newbigging, W.C.W. Chan, *Small* **6**, 138–144 (2010)
11. C. Xie, D. Yin, J. Li, L. Zhang, B. Liu, M. Wu, *Nano Biomed. Eng.* **1**, 39–47 (2009)
12. D. Yin, L. Zhang, C. Xie, B. Liu, L. Zhang, *Nano Biomed. Eng.* **2**, 62–68 (2010)
13. S.P. Low, N.H. Voelcker, L.T. Canham, K.A. Williams, *Biomaterials* **30**, 2873–2880 (2009)
14. M. Vallet-Regí, *J. Intern. Med.* **267**, 22–43 (2010)
15. M.C. Anderson, R. Olsen, *J. Biomed. Mater. Res. Part A* **92**, 1598–1605 (2010)
16. K.J. Nash, P.D.J. Calcott, L.T. Canham, R.J. Needs, *Phys. Rev. B* **51**, 17698 (1995)
17. V. Lehmann, U. Gosele, *Appl. Phys. Lett.* **58**, 856–858 (1991)
18. G. Amato, *Jpn. J. Appl. Phys.* **34**, 1716–1722 (1995)
19. G. Amato, G.D. Francia, P. Menna, D. Ninno, *Europhys. Lett.* **25**, 471–476 (1994)
20. E. Garrone, F. Geobaldo, P. Rivolo, G. Amato, L. Boarino, M. Chiesa, E. Giamello, R. Gobetto, P. Ugliengo, A. Viale, *Adv. Mat.* **17**, 528–531 (2005)
21. J. Park, L. Gu, G. von Maltzahn, E. Ruoslahti, S.N. Bhatia, M.J. Sailor, *Nat. Mater.* **8**, 331–336 (2009)
22. V. Morazzani, J.J. Ganem, J.L. Cantin, in *Structural and Optical Properties of Porous Silicon Nanostructures* (Gordon and Breach Science Publishers, Amsterdam, The Netherlands, 1997). ISBN 90-5699-604-5
23. B.E. Deal, M. Sklar, A.S. Grove, E.H. Snow, *J. Electrochem. Soc.* **114**, 266–274 (1967)
24. A. Mayne, S. Bayliss, P. Barr, M. Tobin, L. Buckberry, *Phys. Stat. Sol. (a)* **182**, 505–513 (2000)
25. S.P. Low, N.H. Voelcker, L.T. Canham, K.A. Williams, *Biomaterials* **30**, 2873–2880 (2009)
26. J.F. Popplewell, S.J. King, J.P. Day, P. Ackrill, L.K. Fifield, R.G. Cresswell, M.L. di Tada, K. Liu, *J. Inorg. Biochem.* **69**, 177–180 (1998)
27. K. Fujioka, M. Hiruoka, K. Sato, N. Manabe, R. Miyasaka, S. Hanada, A. Hoshino, R.D. Tilley, Y. Manome, K. Hirakuri, K. Yamamoto, *Nanotechnology* **19**, 415102 (2008)